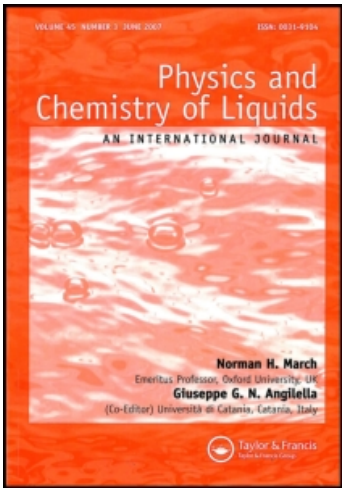

Physics and Chemistry of Liquids
Publication details, including instructions for authors and subscription information:
http://www.informaworld.com/smpp/title~content=t713646857

Atomic distributions in liquid copper-tin alloys

D. M. North[ab]; C. N. J. Wagner[a]
[a] Becton Center Yale University, New Haven, Connecticut [b] Pilkington Brothers Ltd., Research and Development Laboratories Lathom, Ormskirk, Lancashire, England

To cite this Article North, D. M. and Wagner, C. N. J.(1970) 'Atomic distributions in liquid copper-tin alloys', Physics and Chemistry of Liquids, 2: 2, 87 — 113
To link to this Article: DOI: 10.1080/00319107008084082
URL: http://dx.doi.org/10.1080/00319107008084082

Physics and Chemistry of Liquids. 1970. Vol. 2, pp. 87–113

Printed in Great Britain

Atomic Distributions in Liquid Copper-Tin Alloys†

D. M. NORTH‡ and C. N. J. WAGNER

Becton Center
Yale University
New Haven, Connecticut

Abstract—Molten copper–tin alloys have been studied by X-ray diffraction, using a focusing theta-theta diffractometer and Mo–Kα radiation (monochromator in the diffracted beam). Five alloys with 20, 35, 45, 55 and 78 atomic percent Sn, and pure Cu and Sn were measured at temperatures about 20 °C above the liquidus, and at 1100 °C. The total interference functions $I(K)$, where $K = 4\pi \sin\theta/\lambda$, were obtained from the observed scattered intensities $I_a(K)$ per atom and the theoretical atomic scattering factors. Splitting of the first peak in $I(K)$ has been observed in the Cu-55 at% Sn alloy at the liquidus temperature.

The partial interference functions $I_{ij}(K)$ at the liquidus temperature and at 1100 °C were evaluated (assuming that they are independent of atomic concentration) using the five total $I(K)$ of the alloys. The functions $I_{ij}(K)$ are in reasonable agreement with those obtained by Enderby, North and Egelstaff from neutron diffraction data of a Cu-45 at% Sn alloy.

The reduced partial distribution functions $G_{ij}(r) = 4\pi\rho_0 r\{g_{ij}(r) - 1\}$ and the probability functions $g_{ij}(r) = \rho_{ij}(r)/c_j\rho_0$, where $\rho_{ij}(r)$ is the number of j-type atoms per unit volume at the distance r from an i-type atom, c_j is the atomic fraction of j-type atoms and ρ_0 is the average atomic density, have been evaluated by Fourier transformation of $\{I_{ij}(K) - 1\}K$.

The electrical resistivities ρ_R of the alloys, calculated with the Faber–Ziman equation using the measured $I_{ij}(K)$ and Animalu–Heine pseudo-potential elements $U_i(K)$, are in good agreement with the experimental values of Roll and Motz. Assuming that $U_i(2k_F)$ is independent of the values of the Fermi diameter $2k_F$ of the alloys, the concentration dependence of $(3 - X)\rho_R$, where X is the thermoelectric parameter measured by Enderby and Howe, is well reproduced when using the X-ray values of $I_{ij}(2k_F)$.

1. Introduction

The X-ray or neutron scattering patterns of liquid binary alloys are characterized by the three partial interference functions $I_{ij}(K)$.

† Research supported by the United States Atomic Energy Commission.

‡ Present address: Pilkington Brothers Ltd., Research and Development Laboratories, Lathom, Ormskirk, Lancashire, England.

On neglecting the small angle scattering term given by the more complete diffraction theory,[1,2] the scattered intensity per atom $I_a(K)$, where $K = 4\pi \sin\theta/\lambda$ can then be expressed as:

$$I_a(K) = \langle f^2 \rangle - \langle f \rangle^2 + \sum_i \sum_j c_i c_j f_i f_j I_{ij}(K), \tag{1}$$

where f_i is the atomic scattering factor of element i, $\langle f \rangle$ and $\langle f^2 \rangle$ are the mean and mean square scattering factor, respectively, and c_i is the concentration of i. The total interference function, defined as:

$$I(K) = \{I_a(K) - (\langle f^2 \rangle - \langle f \rangle^2)\}/\langle f \rangle^2, \tag{2}$$

is then the weighted sum of the partial interference functions $I_{ij}(K)$. In the case of a binary alloy we can write:

$$I(K) = w_{11} I_{11}(K) + w_{22} I_{22}(K) + 2w_{12} I_{12}(K), \tag{3}$$

where w_{ij} is the weighting factor, which in general is a function of K, i.e.,

$$w_{ij}(K) = c_i c_j f_i(K) f_j(K)/\langle f(K) \rangle^2 \tag{4}$$

In order to determine $I_{ij}(K)$ one needs, in principle, three total interference functions.[3] In neutron diffraction experiments, Enderby, North and Egelstaff[4] varied the scattering power of Cu (i.e., f_j in Eq. (4)) in a liquid Cu-45 at% Sn alloy by isotope enrichment (i.e., using Cu^{63}, Cu^{65} and natural Cu) and solved Eq. (3) for $I_{ij}(K)$. Because of the small intensity differences, particularly between the scattering patterns $I(K)$ of the Cu^{63} and natural Cu alloys, the calculated $I_{ij}(K)$ showed large fluctuations.

Using the X-ray diffraction pattern of Cu-45 at% Sn measured by Orton and Williams as a guide, and together with some additional constraints on the values obtained for the $I_{ij}(K)$, imposed by the fact that $I_a(K)$ is always positive, Enderby *et al.*[4] were able to deduce a final set of values for $I_{ij}(K)$ which reproduced the total interference functions fairly well. Assuming that $I_{ij}(K)$ were independent of concentration, they could predict[6] the X-ray pattern of the Cu-25 at% Sn alloy which agreed quantitatively with that measured by Orton and Williams.[5]

The above assumption of concentration independence of $I_{ij}(K)$ was used to evaluate the partial functions in the liquid Ag–Sn

alloys[2] and in the liquid Au–Sn alloys.[7] In both alloy systems, the partial functions due to Ag–Ag, or Au–Au, and Sn–Sn pairs resembled those of the corresponding pure elements. The partial function due to Ag–Sn pairs lay in between those of the Ag–Ag and Sn–Sn pairs, but the first two peaks in $I_{AgSn}(K)$ were closer to those observed in $I_{AgAg}(K)$ than to the first two peaks in $I_{SnSn}(K)$. The hard sphere model[8,9] predicts that $I_{12}(K)$ falls midway between $I_{11}(K)$ and $I_{22}(K)$. In the case of the Au–Sn alloys, the partial function $I_{AuSn}(K)$ resembled closely a model structure[10] based on a solid AuSn alloy with NiAs-type structure.

However, since partial interference functions have only rigorously been derived for Cu_6Sn_5, it was felt that in order to really test the concentration independence idea an analysis of X-ray scattering data from a number of Cu–Sn alloys could be performed. Alloys of Cu–Sn have previously been measured by Orton and Williams[5] using CuKα radiation ($\lambda = 1.54$ A). In order to extend the data in momentum space K to larger values which are needed for further Fourier transformation, we have used MoKα radiation ($\lambda = 0.71$ A) which yields intensity data between $K = 1.5$ A^{-1} and $K = 15$ A^{-1}. The experimental interference functions $I(K)$ were subsequently used to calculate the partial interference functions $I_{ij}(K)$ and compared with those obtained by Enderby, North and Egelstaff[4] from neutron scattering data of a Cu-45 at% Sn alloy. The partial pair probability functions $g_{ij}(r)$ were then evaluated by Fourier transformation of the $I_{ij}(K)$ obtained from the X-ray data. Applying the electron transport theory of Faber and Ziman,[11] the electrical resistivity and thermo-electric power have been calculated using the experimental $I_{ij}(K)$ and the Animalu–Heine[12] pseudopotential elements.

2. Experimental Procedure

Alloys of Cu and Sn with 20, 35, 45, 55, and 78 atomic percent (at%) Sn were prepared in a graphite crucible directly in the X-ray high temperature camera. Some reasons for the choice of these alloys are given. In the vicinity of 20% Sn the experimental resistivity is seen to exhibit a maximum. The 45% Sn alloy obviously corresponds to the composition investigated with neutrons; whilst the 78% Sn alloy should exhibit a split first peak in $I(K)$ if concentra-

tion independence holds and if investigated with neutrons for natural Cu; though this latter postulate has not yet been verified. The other two alloys simply add a composition balance to the investigations.

The X-ray diffraction patterns of the liquid alloys, and of pure copper and tin were recorded in the range of $2\theta = 8°$ to $2\theta = 120°$ on a theta–theta diffractometer[13,14] using MoKα radiation and a bent LiF monochromator in the diffracted beam. A series of measurements were carried out in a He-20% H atmosphere with each sample at temperatures about 20 °C above the liquidus, and another series at 1100 °C.

The raw intensity data were corrected for polarization and absorption, and then converted to absolute intensities $I_a(K)$ per atom expressed in electron units using the high angle and RDF normalization procedure,[15] with the atomic scattering factors of Cu and Sn calculated by Cromer and Waber,[16] corrected for dispersion,[17] and the Compton scattering as given by Sagel.[18]

The total interference functions $I(K)$ were calculated from $I_a(K)$ using Eq. (2). $I(K)$ were refined in such a way that the corresponding Fourier transforms, i.e., the reduced total distribution functions

$$G(r) = 4\pi r\{\rho(r) - \rho_0\} = (2/\pi)\int_0^\infty K\{I(K) - I\} \sin Kr \, dK, \qquad (5)$$

where ρ_0 is the average atomic density of the alloy, and $4\pi r^2\rho(r)$ is the radial distribution function (RDF), were equal to $-4\pi\rho_0 r$ for values of r less than the interatomic distances in the alloys. The refined $I(K)$ of the alloys with 20, 35, 45, 55 and 78 at% Sn were then used to calculate $I_{CuCu}(K)$, $I_{SnSn}(K)$ and $I_{CuSn}(K)$ by a least square analysis.[2]

The partial interference functions $I_{ij}(K)$ were finally Fourier transformed to obtain the reduced partial distribution functions $G_{ij}(r) = 4\pi\rho_0 r\{g_{ij}(r) - 1\}$ and the partial pair distribution functions $g_{ij}(r) = \rho_{ij}(r)/c_j\rho_0$, where $\rho_{ij}(r)$ is the number of j-type atoms per unit volume at the distance r from an i-type atom, i.e.,

$$I_{ij}(K) = 1 + \frac{4\pi\rho_0}{K}\int_0^\infty r\{g_{ij}(r) - 1\} \sin Kr \, dr \qquad (6)$$

and

$$G_{ij}(r) = 4\pi\rho_0 r\{g_{ij}(r) - 1\} = (2/\pi)\int_0^\infty K\{I_{ij}(K) - 1\} \sin Kr\, dK \quad (7)$$

or

$$g_{ij}(r) = 1 + \frac{1}{2\pi^2\rho_0 r}\int_0^\infty K\{I_{ij}(K) - 1\} \sin Kr\, dK \quad (8)$$

The normalization of the data, the calculation of $I(K)$ and $G(r)$, the least square analysis to obtain $I_{ij}(K)$, the calculation of $G_{ij}(r)$, and the refinement procedure were handled with computer programs[19] written in FORTAN IV.

3. Experimental Results

A. Total Interference Functions

The interference functions $I(K)$ of Cu and Sn are shown in Fig. 1, and the total interference functions of the Cu–Sn alloys are shown in Figs. 2(a) and 2(b), measured at the temperatures indicated in the diagrams (approximately 20 °C above the liquidus), and in Figs. 3(a) and 3(b), measured isothermally at 1100 °C.

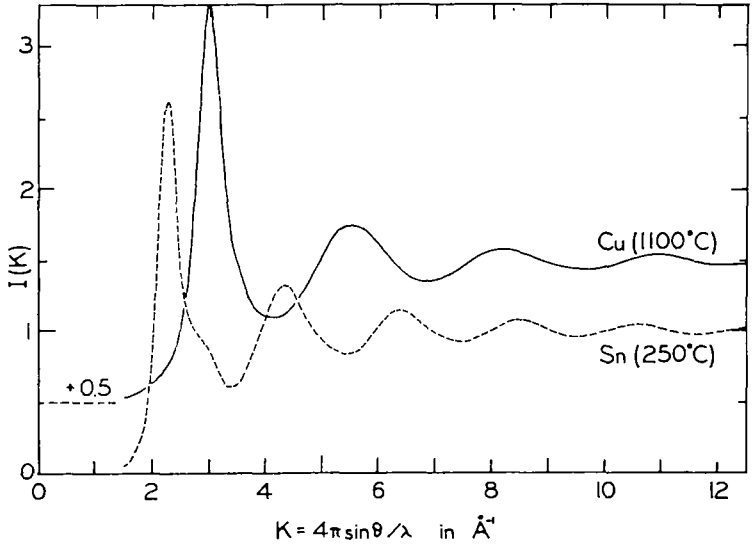

Fig. 1. Interference functions of liquid copper and tin.

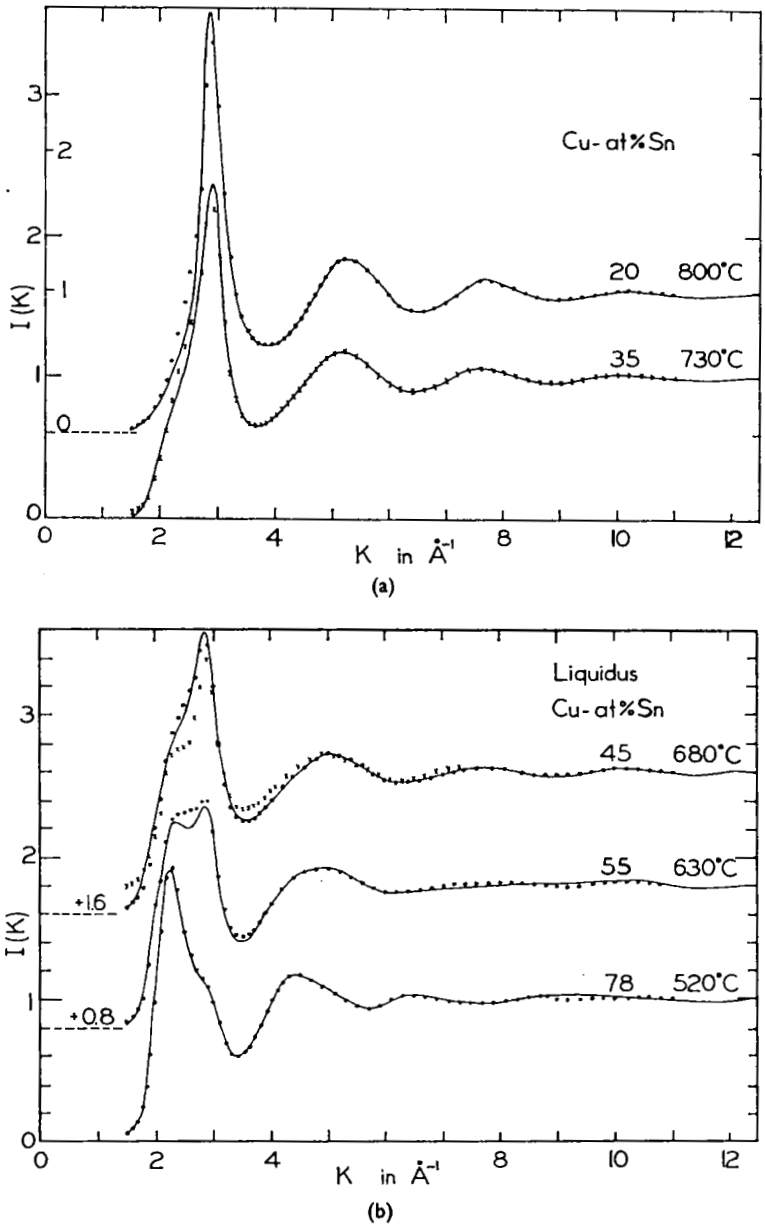

Fig. 2. Total interference functions of Cu–Sn alloys, measured at 20 °C above the liquidus. The solid lines represent the experimental data. The circles and crosses represent $\sum_i \sum_j w_{ij} I_{ij}(K)$, calculated with the X-ray data, with the exception of the 45 at% curve where the crosses represent a calculation with the neutron $I_{ij}(K)$.

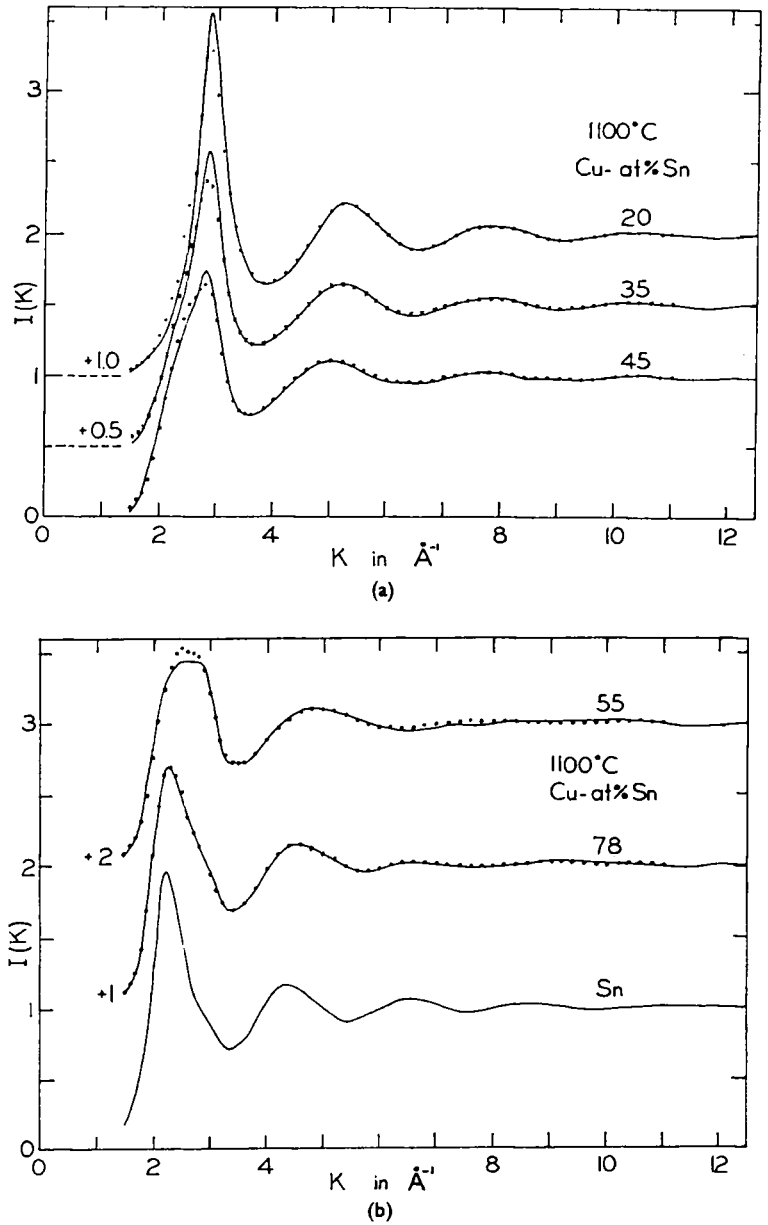

Fig. 3. Total interference functions of Cu–Sn alloys, measured at 1100 °C. The solid lines represent the experimental data. The circles and crosses represent $\sum_i \sum_j w_{ij} I_{ij}(K)$.

The interference functions of Cu and Sn differ from those published previously[14] which should be considered of lower accuracy. The large surface tension of Cu previously caused the liquid sample to form practically a hemi-sphere in the graphite crucible (one square inch) which leads to an absorption error at low angles. In order to obtain a fairly flat sample a molybdenum boat was used in the present investigation of liquid Cu as suggested by Ruppersberg.[20]

Sn and the alloys of Cu–Sn were contained in a graphite boat during the X-ray measurements. The addition of Sn to Cu lowered the surface tension enough to yield samples of relatively flat surfaces (about one square centimeter) in the graphite crucibles. The interference function of liquid Sn measured at 250° is in very good agreement with the recent reflection X-ray data of Kaplow *et al.*,[10] the transmission X-ray data of North and Wagner[21] and the neutron data of North *et al.*[22] Our results for liquid Cu also agree fairly well with some recent neutron work by Breuil and Tourand.[37]

The interference functions of the alloys, shown in Fig. 2 at the liquidus temperature, with 35 and 45 at% Sn show a shoulder at the low angle side of the first peak in $I(K)$. A splitting of the first peak is observed in the Cu-55 at% Sn alloy, whereas the alloy with 78 at% Sn exhibits a shoulder on the high angle side of the first peak, more pronounced than that observed in pure Sn. These results are in reasonable agreement with those of Orton and Williams[5] who measured Cu–Sn alloys with 16, 20, 25, 45, 56, and 68 at% using Cu radiation in the range between $K = 1.5$ A^{-1} and 6.5 A^{-1}.

The effect of temperature on the interference functions of the alloys and pure Sn (Fig. 3) is to reduce the height of the peaks and to broaden them. This is most clearly seen on the first peak where only shoulders or a rather flat peak maximum (in the case of the Cu-55 at% Sn) are observed.

In both series of measurements the alloys with 45, 55 and 78 at% Sn show only the first two peaks clearly outside the scatter of the experimental data points whose error bars are of the order of ± 0.02 beyond $K = 6$ A^{-1}, ± 0.05 over the second peak, and ± 0.10 over the first peak.

B. Partial Interference Functions

Assuming that they are independent of the relative abundance

of the elements in the alloys, $I_{CuCu}(K)$, $I_{CuSn}(K)$, and $I_{SnSn}(K)$ were calculated by a least square analysis using the total interference functions $I(K)$ of the alloys with 20, 35, 45, 55, and 78 at% Sn. Figure 4 shows the partial interference functions $I_{ij}(K)$ obtained from $I(K)$ of the alloys measured at the liquidus temperature, and Fig 5 shows $I_{ij}(K)$ at 1100 °C. Both sets of partials are rather similar in shapes and positions; only the height of the first peak is reduced as a consequence of the increased temperature.

In order to show to what extent $I_{ij}(K)$, calculated with the X-ray data by a least square analysis, are able to reproduce the original $I(K)$ of the alloys, the weighted sums of the three $I_{ij}(K)$ (Eq. (3)) are represented as dots or crosses in Figs. 2 and 3. However, in Fig. 2, for the 45 at% Sn alloy, the crosses represent a calculation using the $I_{ij}(K)$ evaluated from the neutron experiments of Enderby *et al.*[4] The agreement between measured and calculated $I(K)$ is reasonable.

C. Pair Distribution Functions

The reduced partial distribution functions $G_{ij}(r)$ and the partial pair distribution functions $g_{ij}(r)$, calculated by Fourier transformation of $I_{ij}(K)$ (Eqs. (6), (7) and (8)), are shown in Figs. 6 and 7 for the liquidus temperature, and in Figs. 8 and 9 for 1100 °C. The position r_1 of the first peak maximum of $g_{ij}(r)$ is a measure of the interatomic separation between ij atom pairs. The values of $(r_1)_{CuCu}$, $(r_1)_{SnSn}$ and $(r_1)_{CnSn}$ are given in Table 2. The partial radial distribution functions (RDF) $4\pi r^2\rho_{ij}(r)/c_j$ allow us to determine the coordination number η_{ij}, i.e.,

$$\eta_{ij} = \int_{r_0}^{r_2} 4\pi r^2\{\rho_{ij}(r)/c_j\}\,dr, \tag{9}$$

where r_0 is the value of r below which the RDF is zero and r_2 is the position of the first minimum of the RDF. The value $\eta_{SnSn} = 9$ corresponds closely to that observed in pure, liquid Sn, whereas $\eta_{CuCu} = \eta_{CuSn} = 13$ are larger than those of close packed liquid metals such as Ag or Cu.

The reduced distribution functions $G(r)$ (Eq. (6)) of pure Cu and Sn, and of the alloys are shown in Figs. 10 and 11. It is easily seen that $G_{Cu}(r)$ and $G_{Sn}(r)$ resemble $G_{CuCu}(r)$ and $G_{SnSn}(r)$, respectively.

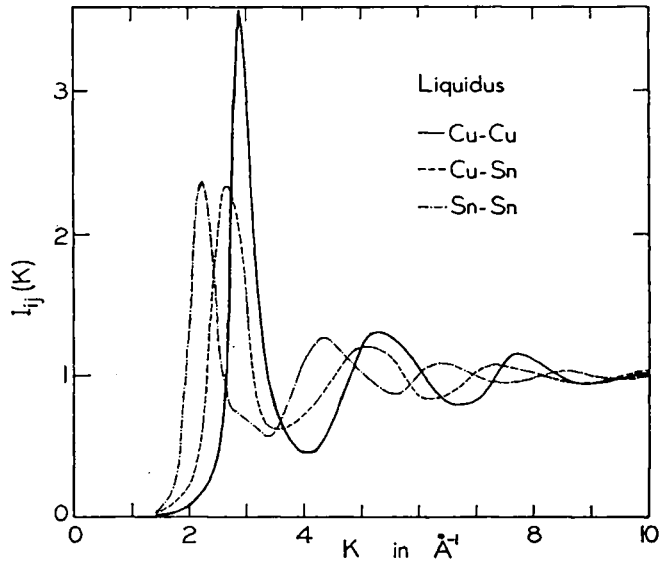

Fig 4. Partial interference functions (structure factor) $I_{ij}(K)$ in liquid Cu–Sn at the liquidus temperatures.

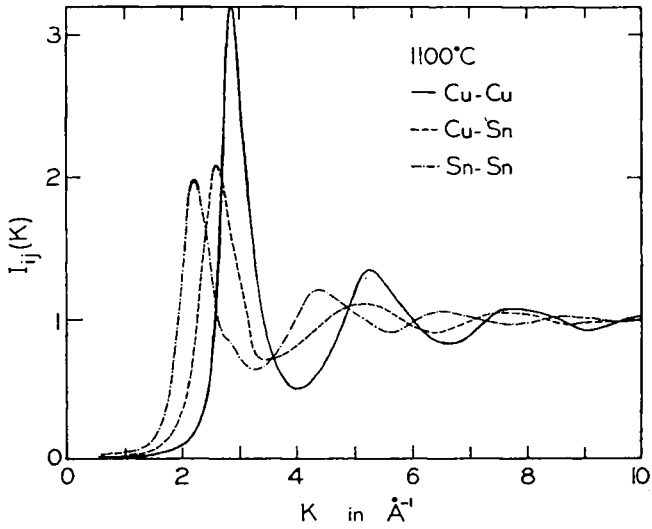

Fig. 5. Partial interference functions (structure factor) $I_{ij}(K)$ in liquid Cu–Sn, at 1100 °C.

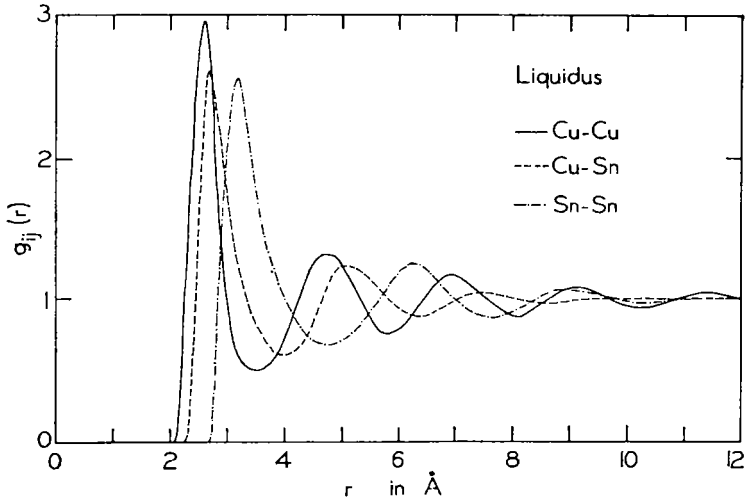

Fig. 6. Partial pair distribution functions $g_{ij}(r)$ in liquid Cu–Sn (liquidus).

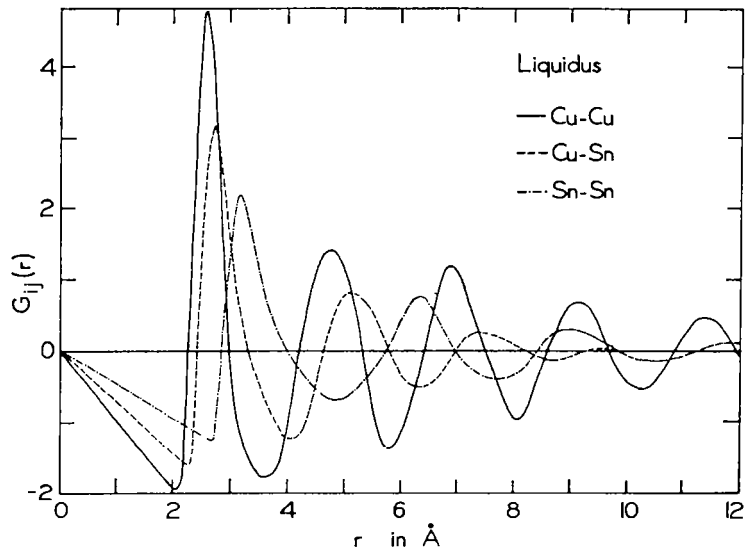

Fig. 7. Reduced partial distribution functions $G_{ij}(r) = 4\pi r\rho_o\{g_{ij}(r) - 1\}$ in liquid Cu–Sn (liquidus).

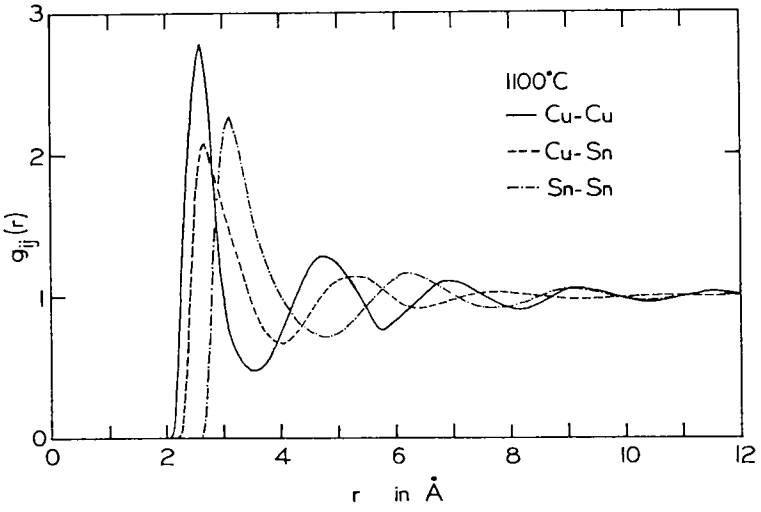

Fig. 8. Partial pair distribution functions $g_{ij}(r)$ in liquid Cu–Sn (Isothermal).

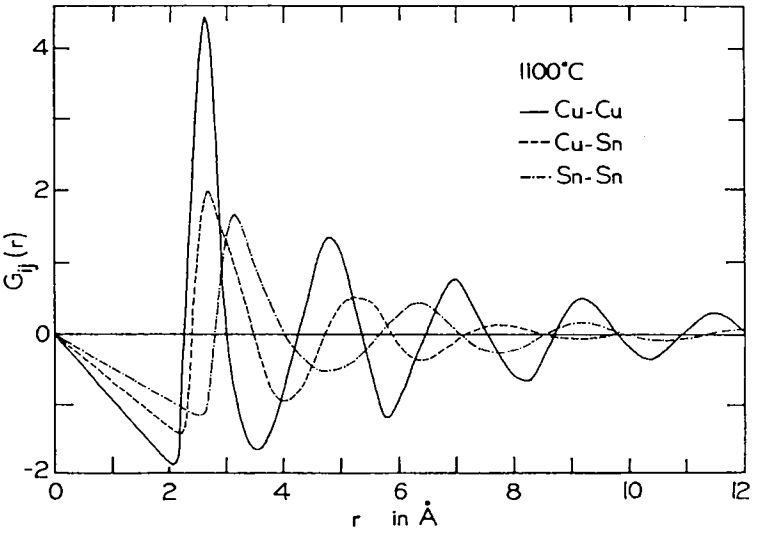

Fig. 9. Reduced partial distribution functions $G_{ij}(r) = 4\pi r\rho_0\{g_{ij}(r) - 1\}$ in liquid Cu–Sn (Isothermal).

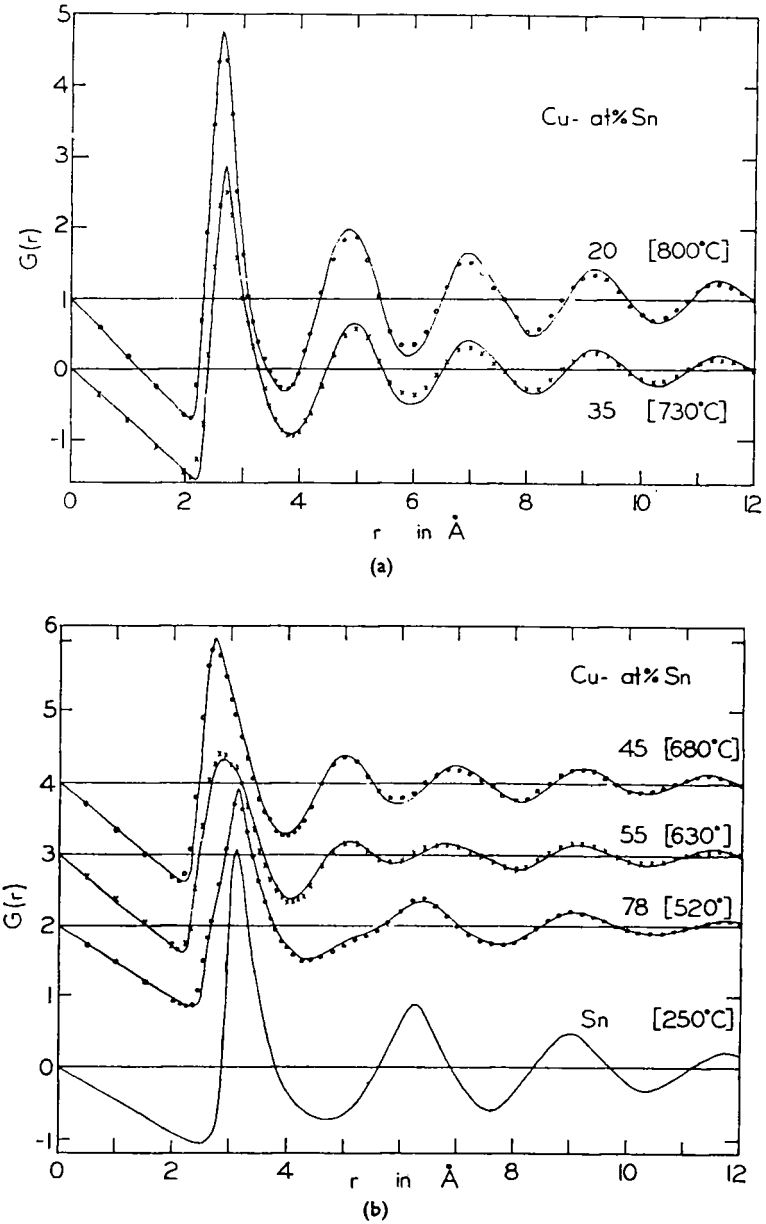

Fig. 10. Reduced total distribution functions $G(r)$ of liquid Cu–Sn alloys at the liquidus. The solid lines represent the Fourier transforms of $K\{I(K) - 1\}$. The circles and crosses represent $\sum_i \sum_j w_{ij} G_{ij}(r)$.

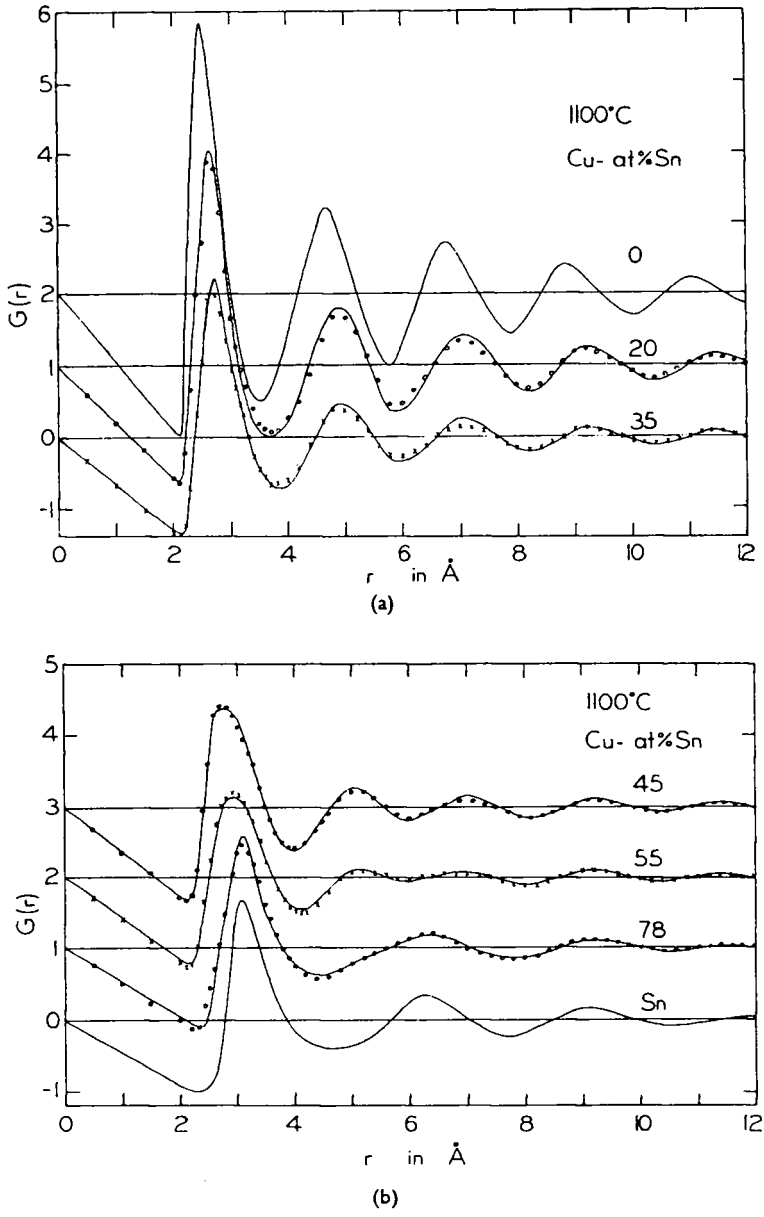

Fig. 11. Reduced total distribution functions $G(r)$ of liquid Cu–Sn alloys at the isothermal. The lines, circles and crosses represent the same parameters as for Fig. 10.

But $(r_1)_{Cu}$ is slightly smaller then $(r_1)_{CuCu}$, a difference which is believed to be outside the error of the experimental data.

D. Electronic Transport Properties

The electrical resistivity ρ_R and the thermoelectric power Q were calculated using the relations given by Faber and Ziman,[11] i.e.,

$$\rho_R = \{(\pi^3\hbar Z)/(e^2k_F)\} \langle | V(K) |^2 \rangle \tag{10}$$

and

$$Q = -\{(\pi^2k_B{}^2T)/(3 | e | E_F)\} X, \tag{11}$$

where

$$\langle | V(K) |^2 \rangle = 4 \int_0^1 | V(K) |^2 (K/2k_F)^3 \, d(K/2k_F), \tag{12}$$

$$| V(K) |^2 = \langle U^2 \rangle - \langle U \rangle^2 + \sum_i \sum_j c_i c_j U_i(K) U_j(K) I_{ij}(K), \tag{13}$$

and X is the thermoelectric parameter:

$$X = 3 - 2 | V(2k_F) |^2 / \langle | V(K) |^2 \rangle \tag{14}$$

In the above expressions, Z is the effective valence of the alloy, which is taken to be free electron like, k_F and E_F are the Fermi radius and energy, respectively, k_B is the Boltzmann constant, and T is the absolute temperature. The pseudo-potential elements $U_i(K)$ used in Eq. (13) are dimensionless, and have been normalized so that

$$U_i(0) = -Z_i/Z, \tag{15}$$

where Z_i is the valency of the element concerned. They have been derived from Animalu–Heine pseudopotentials[12] $U_i{}^{AH}(K)$ for pure elements such that[23]

$$U_i(K) = U_i{}^{AH}(K) \, Z_i/\{(2E_F/3)_i Z\} \tag{16}$$

The electrical resistivities ρ_R are plotted in Fig. 12 using the partial interference functions $I_{ij}(K)$ of Figs. 4 and 5. Also shown are the experimental values of Roll and Motz.[24]

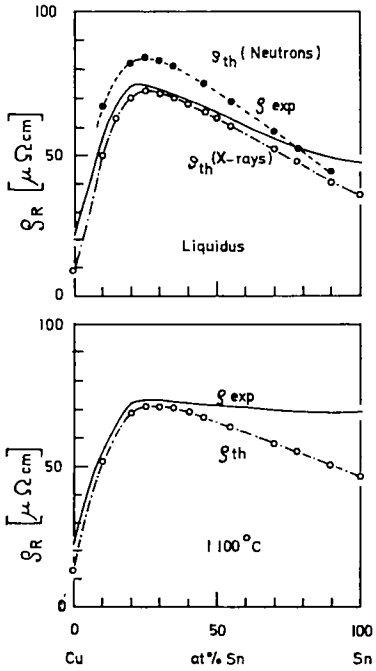

Fig. 12. Concentration dependence of the experimental and theoretically predicted electrical resistivities of Cu–Sn alloys at the liquidus and at 1100 °C.

4. Discussion

A. Interference Function

The total interference functions of the Cu–Sn alloys, shown in Figs. 2 and 3, resemble those of Au–Sn.[7,10] In both systems, one observes a splitting of the first peak in $I(K)$, for an alloy with about 60 at% Sn (in Cu and Au, respectively), whereas only a broadening of the first peak is found in Ag–Sn alloys.[2] This is due to the fact that the positions of the maxima and minima in $I_{ij}(K)$ do not coincide, and the scattering amplitudes f_1 and f_2 differ appreciably for Cu and Sn, but not enough in the case of Ag–Sn. In addition the separation between the first peak of $I_{11}(K)$ and $I_{22}(K)$ is much greater in Cu–Sn than in Ag–Sn. Although $I_{11}(K)$ and $I_{22}(K)$ are almost identical for Ag–Sn[2] and Au–Sn[7], we do observe a splitting of the first peak in $I(K)$ for a Au-67 at% Sn alloy,[7] which is a

consequence of the superposition of the first peak of $I_{AuAu}(K)$ and $I_{AuSn}(K)$,[7] in addition to the difference in f_{Au} and f_{Sn}.

The partial interference functions $I_{ij}(K)$ of Cu–Sn alloys obtained by the least square analysis of the X-ray data are in reasonable agreement with those of Enderby *et al.*[4] obtained from neutron data of a Cu-45 at% Sn alloy (Fig. 13). When comparing the X-ray and

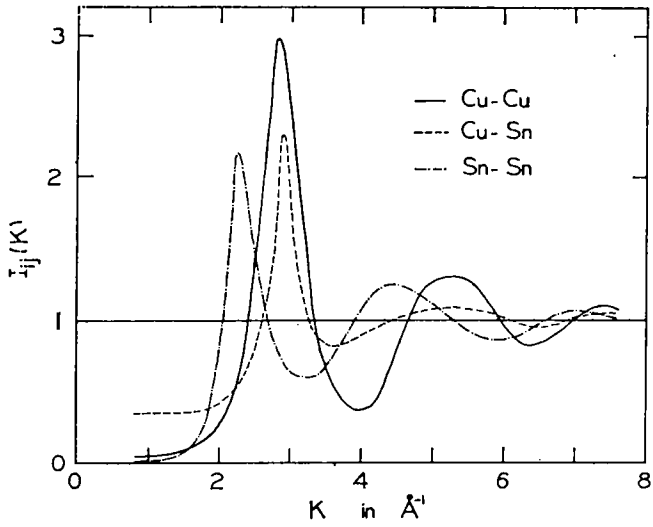

Fig. 13. Partial interference functions in Cu–Sn alloys evaluated from the neutron experiments of Enderby, North and Egelstaff.[4]

neutron partial functions (Figs. 4, 5 and 13), it is seen that both $I_{CuCu}(K)$ and both $I_{SnSn}(K)$ are quite similar. The positions K_n of the first two maxima in $I_{ij}(K)$ agree very well as shown in Table 1. The only discrepancy exists between the position K_1 of the first peak in $I_{CuSn}(K)$, whereas both K_2 are almost identical.

It should be emphasized that the evaluation of that part of the partial functions $I_{ij}(K)$ corresponding to the first peak from the X-ray or neutron total interference functions is very difficult and uncertain. Any error in position and intensity of these peaks in the original data will drastically affect the partial functions because of the relative sharpness of the first maximum compared to the broader and smaller peaks at larger K values. Only by imposing additional, necessary and sufficient conditions governing quadratic functions

TABLE 1 Positions K_n in Å^{-1} of the First Three Maxima of the Interference Functions of Cu, Sn, Cu–Cu, Cu–Sn and Sn–Sn. The Neutron Figures for Cu are taken from Breuil and Tourand[37] and for Sn from North *et al.*[22]

	X-rays			Neutrons	
	K_1 [Å^{-1}]	K_2 [Å^{-1}]	K_3 [Å^{-1}]	K_1 [Å^{-1}]	K_2 [Å^{-1}]
Cu–Cu	2.90	5.35	7.75	2.85	5.3
Cu–Sn	2.70	5.15	7.4	2.90	5.2
Sn–Sn	2.25	4.35	6.4	2.25	4.4
Cu	3.00	5.50	8.2	3.00	5.52
Sn	2.25	4.35	6.4	2.21	4.30

and using the X-ray interference function of Orton and Williams[5] were Enderby *et al.*[4] able to deduce meaningful partial functions particularly in the vicinity of the first peaks. The X-ray partial functions, however, represent the values obtained by a least square analysis of all intensity data of the alloys without imposing any additional conditions.

The real test about the usefulness of the X-ray or neutron partial functions rests in their reproduction of the X-ray and neutron total interference function of the Cu-45 at% Sn alloy, using Eq. (3). As can be seen from Fig. 2, the weighted sum of the X-ray $I_{ij}(K)$ reproduces the X-ray total $I(K)$ fairly well. The same holds true for the sum of the neutron $I_{ij}(K)$ beyond the first peak. Only the low angle side of the first peak does not agree with our X-ray data, and we believe that this is a consequence of the use of the data of Orton and Williams[5] by Enderby *et al.*[4] which are appreciably lower than our own results over the first peak. Conversely, however, the X-ray $I_{ij}(K)$ lead to a fairly good agreement with the neutron $I(K)$ of the Cu-45 at% Sn alloy, as shown in Fig. 14 for the $I(K)$ obtained with natural Cu and Sn.

The partial interference functions $I_{ij}(K)$ of the Cu–Sn system resemble in many respects the $I_{ij}(K)$ of Ag–Sn alloys. $I_{SnSn}(K)$ and $I_{12}(K)$, where the subscripts represent Cu–Sn and Ag–Sn, respectively, possess a first maximum of about equal height, but $I_{11}(K)$ is higher than $I_{12}(K)$. The position of K_1 of $I_{12}(K)$ falls in between those of $I_{11}(K)$ and $I_{SnSn}(K)$, and is somewhat closer to K_1 of the

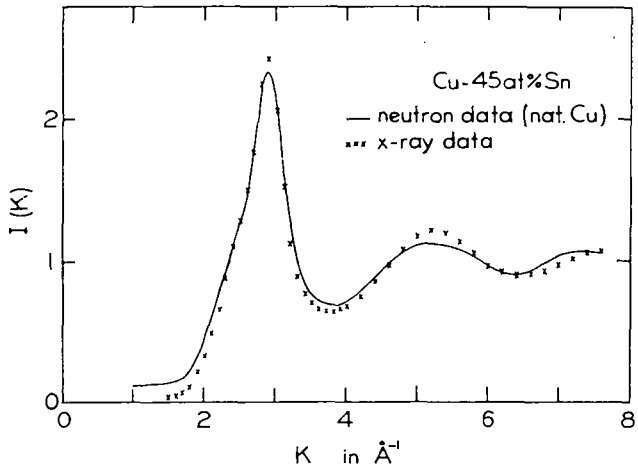

Fig. 14. Comparison between the neutron $I(K)$ of liquid Cu-45 at% Sn and the $I(K)$ calculated with the X-ray $I_{ij}(K)$.

$I_{11}(K)$ peaks. This represents only a slight deviation from what would be expected from the hard sphere model.[6,8,9]

In contrast to the Ag–Sn and Au–Sn alloys, where the partial interference functions $I_{AgAg}(K)$ and $I_{AuAu}(K)$ resembled very closely the interference functions of the pure liquid Ag[2] and Au,[25] respectively, the partial function $I_{CuCu}(K)$ does not coincide with $I(K)$ of pure liquid Cu as can be seen from Figs. 1, 4, and 5. The positions K_n of the maxima of $I_{CuCu}(K)$ are smaller than those of $I_{Cu}(K)$, i.e., $K_1(\mathrm{CuCu}) = 2.90\ \mathrm{A}^{-1}$ and $K_1(\mathrm{Cu}) = 3.00\ \mathrm{A}^{-1}$ (Table 1). The partial function $I_{SnSn}(K)$, however, resembles that of $I_{Sn}(K)$ as found previously for the Ag–Sn and Au–Sn systems.

In passing we may add that attempts were also made to extract partials firstly from the three neutron curves and our X-ray result for Cu-45 at% Sn, and secondly from just a combination of four out of the five X-ray curves. However, the initial set of partials that were generated indicated that major trial and error calculations would have had to be performed in order to obtain a final set of smoothly varying partials that could be summed to produce the original intensity data. This appears to be in accordance with the conclusions of Enderby *et al.*[4] that the more intensity patterns (that

sufficiently differ from each other) available for analysis the better for a rapid convergence of the partials.

B. Distribution Functions

The partial, reduced distribution functions $G_{ij}(r)$ (Figs. 7 and 9) and the partial pair distribution functions $g_{ij}(r)$ (Figs. 6 and 8) allow us to determine the interatomic distances in the alloys. As shown in Table 2, the values r_n of all maxima of $G_{CuCu}(r)$ appear at

Table 2 Values of the Position r_n in Å of the First and Second Peak Maxima of $G_{ij}(r)$ and $G(r)$.

Composition	Liquidus		1100 °C	
	r_1[Å]	r_2[Å]	r_1[Å]	r_2[Å]
Cu–Cu	2.60	4.8	2.60	4.8
Cu–Sn	2.70	5.2	2.67	5.3
Sn–Sn	3.14	6.3	3.10	6.3
Cu–0 at% Sn	2.50	4.7	2.50	4.7
–20	2.65	4.85	2.65	4.9
–35	2.70	5.0	2.70	5.0
–45	2.76	5.0	2.76	5.0
–55	2.95	(5.1)	2.95	(5.1)
–78	3.12	(6.4)	3.10	(6.4)
–100	3.12	6.25	3.08	6.3

slightly larger values of r than those of $G_{Cu}(r)$ as shown in Figs. 7, 9, and 11. This is consistent with the observation in $I(K)$, and indicates that the atomic arrangement about a Cu atom in the alloys is different from that observed in pure Cu, but it is quite similar for the Sn atoms in the Cu–Sn alloys and pure Sn.

It should noted that the values r_n(Cu–Cu) resemble much more closely those of the Cu-20 at% Sn alloy than pure Cu. This seems to indicate that there might be some similarity with the structure of the high temperature phase of Cu_3Sn which possesses a Fe_3 Al-type structure.[26] The distance of closest approach between Cu–Cu and Cu–Sn atoms is about 2.65 A, which is in reasonable agreement with the values of r_1(Cu–Cu) and r_1(Cu–Sn). Such structural order in Cu–Sn alloys is also indicated by the minimum in the heat mixing vs composition curve ($H_M \sim -1$ kcal) at about 25 at% Sn. The

observed co-ordination numbers $\eta_{CuCu} = \eta_{CuSn} = 13$ are also consistent with a Fe_3Al-type structure with 8 nearest and 6 next-nearest neighbours.

The radial distribution functions of pure Cu and Sn are in very good agreement with previous observations.[10,20,27] Only when the upper limit K_{max} in the integral of Eq. (6) is larger than 15 A^{-1} does one observe values of r_1 which are representative of the interatomic distances in the liquid.[28]

The reduced total distribution functions $G(r)$ of the alloys, shown in Figs. 10 and 11, represent the sum of convolution products of $W_{ij}(r)$, which is the Fourier transform of $w_{ij}(K)$ (Eq. (4)), and $G_{ij}(r)$[1,29] i.e.,

$$G(r) = \sum_i \sum_j \int W_{ij}(u)\, G_{ij}(r-u)\, du \tag{17}$$

If, however, $w_{ij}(K)$ is independent of K, i.e. $w_{ij}(K) = w_{ij}$, then $W_{ij}(r) = w_{ij}\,\delta(r)$, where $\delta(r)$ is the Dirac delta function, and Eq. (17) reduces to the well known relation[1,2,10,30]

$$G(r) = \sum_i \sum_j w_{ij}\, G_{ij}(r). \tag{18}$$

In order to test the relation (18), the total reduced distribution functions $G(r)$ of the alloys, calculated from $I(K)$ using Eq. (5) and represented as solid curves in Figs. 10 and 11, were compared with $G(r)$, evaluated with Eq. (18) and represented as open circles or crosses in Figs. 10 and 11. It is obvious from these figures that the agreement between the $G(r)$ curves is excellent, indicating that the partial functions $G_{ij}(r)$ are representative of the distributions of atoms about the Cu and the Sn atoms in the alloys.

It is interesting to note that the total $G(r)$ for certain alloys shows only a prominent first peak, and thereafter very little structure. This is particularly true for the alloy with 55 at% Sn. By just considering the total $G(r)$ it might, quite wrongly, be concluded that this alloy does not show any structural order beyond nearest neighbours. On the contrary, the damping-out of $G(r)$ is the consequence of the fact that the weighted sum of $G_{ij}(r)$ exhibits small oscillations only.

The positions r_1 of the first peak in total $G(r)$ of the alloys has been interpreted as the distance between neighboring atoms in the alloys.

However, it is clear from Eq. (18) that r_1 really represents the position of the first peak maxima of the weighted sum of the three partial distribution functions $G_{ij}(r)$ and will, therefore, be strongly influenced by the weighting factors w_{ij}. The same argument holds true for the co-ordination number η, obtained from $4\pi r^2\rho(r) = rG(r) + 4\pi r^2\rho_0$.

C. Electronic Transport Properties

In these calculations the model pseudopotentials of Animalu and Heine for Sn[12] and Cu[31] have been used together with the partial interference functions of Figs. 4 and 5. In using these pure metal potentials the central assumption made is that they are independent of concentration and electron energy. When using these potentials in the alloys, changes in volume and conduction electron screening should be allowed for, and in an attenpt to do so the potentials were scaled in the manner outlined at Eq. (16). Since changes in screening should really only affect the low K region of the potential, any errors committed by this scaling are in all probability slight, particularly since the resistivity integrands are dominated by the peaks in the partials, with the exception perhaps of the concentrations nearer that of pure Cu.

The calculated electrical resistivities are in good agreement with the experimental values of Roll and Motz[24] at the liquidus temperature, as shown in Fig. 12. At 1100°, the theoretical values of ρ_R are slightly lower than the experimental values at high Sn concentrations. Similar differences have been observed in the Ag–Sn[2] and Au–Sn[7] alloys. However, the overall variation, in particular the initial steep increase, of the electrical resistivity as a function of alloy concentration has been successfully explained with the Faber–Ziman theory,[11,32,33] i.e., the large values of ρ_R at about 20 to 25 at% Sn are a consequence of the proximity of the value of the Fermi diameter $2k_F$ to the positions K_1 of the first peaks in $I_{ij}(K)$. Even the negative temperature coefficient of resistivity of the Cu–Sn alloys in this concentration range, calculated from $I(K)$, agreed rather well with the experimental data.[34]

A more severe test of the Faber–Ziman theory would be the prediction of the concentration dependence of the thermoelectric power, a parameter extremely sensitive to the values of input data at $2k_F$, of the Cu–Sn alloys, which has been measured recently by Enderby

and Howe.[35] These authors have actually plotted $(3-X)\rho_R$ as a function of concentration. It is easily seen by combining Eqs. (10) and (14) that:

$$(3-X)\rho_R = 0.051\frac{Z}{2k_F}|V(2k_F)|^2, \tag{19}$$

where $|V(K)|^2$ is defined in Eq. (13) and $2k_F$ is in A^{-1}. Values of $(3-X)\rho_R$ calculated with the Animalu–Heine pseudopotentials are shown in Fig. 15 (dotted curve), together with the experimental

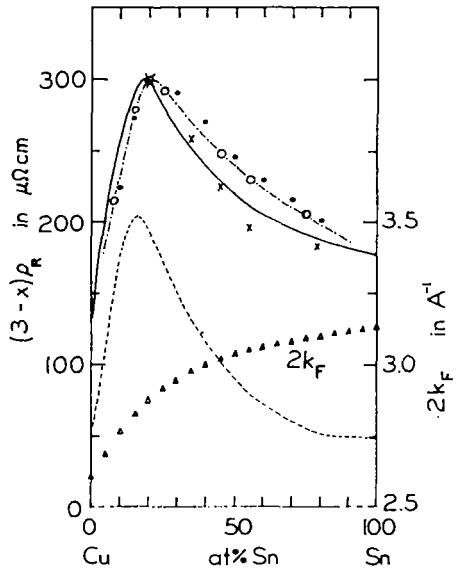

Fig. 15. Concentration dependence of $(3-X)\rho_R$ in Cu–Sn alloys measured at 1100 °C. Solid line represents the experimental data of Enderby and Howe.[35] The predicted values are represented by open circles when using the X-ray values of $I_{ij}(2k_F)$, by solid circles when using the neutron values of $I_{ij}(2k_F)$, and by the crosses when using the X-ray total $I(2k_F)$. Also shown are the values of $2k_F$ as a function of Sn concentration.

values (solid curve) of Enderby and Howe.[35] It is evident that the absolute magnitudes do not agree; but the qualitative features across the concentration range are faithfully reproduced. The actual discrepancy between the experimental and theoretical values of $(3-X)\rho_R$ is probably due to the uncertainties of the pseudopotential elements at $K = 2k_F$.

For this reason, Enderby and Howe[35,36] suggested determining $U(2k_F)$ of Cu and Sn in Eqs. (13) and (19) from the experimental data of $(3-X)\rho_R$. The calculated values of $U(2k_F)$ can then be used to evaluate $(3-X)\rho_R$ (Eq. (19)) assuming that the $2k_F$ dependence of U is much smaller than that of I_{ij}. From the values of $I_{CuCu}(2k_F)$, $I_{SnSn}(2k_F)$ and $(3-X)\rho_R$ of Cu and Sn, all measured at 1100 °C, it follows that $\{U(2k_F)\}^2_{Cu} \simeq \{U(2k_F)\}^2_{Sn} = 4 \times 10^3$. Therefore, Eq. (19) reduces to

$$(3-X)\rho_R = 0.051 \frac{Z}{2k_F} \{| U |^2 (c_1^2 I_{11} + c_2^2 I_{22} + 2c_1 c_2 I_{12})\}_{2k_F} \qquad (20)$$

Values of $(3-X)\rho_R$ calculated with Eq. (20) are also shown in Fig. 15 (open circles) together with the theoretical values (closed circles) of Enderby and Howe[35] who used the neutron partial interference functions of Enderby *et al.*[4] Both sets of data are almost identical and agree rather well with the experimental values. This is a consequence of the fact that $c_1^2 I_{11} + c_2^2 I_{22} + 2c_1 c_2 I_{12}$ of the X-ray and neutron partial interference functions yield almost identical values.

Even if we were to take the values of the total interference function $I(K)$ at $K = 2k_F$ i.e., instead of using $\sum_i \sum_j c_i c_j I_{ij}(2k_F)$ in Eq. (20) we replace it by $\sum_i \sum_j w_{ij} I_{ij} I_{ij}(2k_F)$, we obtain values of $(3-X)\rho_R$ which are also in good agreement with the experimental data, because $I(2k_F)$ is only slightly smaller than $\sum_i \sum_j c_i c_j I_{ij}(2k_F)$.

5. Conclusions

It must be emphasized that the correct procedure to adopt in a structure investigation of an alloy system like Cu–Sn, is to perform for example, an isotope enrichment experiment in the manner of Enderby *et al.*,[4] for each particular composition and temperature involved. However, this sort of experiment is difficult and could be expensive; the analysis becomes tedious and the uncertainties large particularly if three interference patterns only are available. In view of this and the fact that there are only a limited number of systems ideally suited for investigation with the isotope enrichment technique, it would appear that the " concentration independent " experiment with X-rays, given here, offers a most useful alternative with which to investigate a host of alloy systems. In any work on an

alloy one must bear in mind the importance of a size difference, if any, between the atoms involved, because if there is no difference in size then a simple liquid substitutional alloy could result, where the partials are almost identical, and where a detailed analysis as outlined above need never be conducted.

Obviously if " concentration independence "is a valid approximation, then the X-ray and neutron sets of partials should be identical. That they are not identical is not surprising, since on the one hand the X-ray results are representative of a wide concentration range whilst the neutron partials are unique to one composition. However, in view of the large uncertainties in both sets of partials, particularly in the neutron case, one should not place too much emphasis on these differences, and should consider the agreement as being reasonably good.

The X-ray scattering patterns of the Cu–Sn alloys can be easily interpreted as the weighted sum of the partial interference functions $I_{ij}(K)$. Furthermore, for the 45 at% Sn composition, the X-ray $I_{ij}(K)$ reproduce faithfully the neutron total interference function (see Fig. 14), whilst the neutron $I_{ij}(K)$ is in close agreement with the X-ray total $I(K)$ (see Fig. 2). The Fourier transforms of the X-ray $I_{ij}(K)$ yield atomic distribution functions $G_{ij}(r)$ which in turn reproduce very accurately the total distribution function $G(r)$ which is essentially the transform of $I(K)$. Though $I_{\mathrm{SnSn}}(K)$ is seen to be very similar to $I(K)$ for pure Sn, $I_{\mathrm{CuCu}}(K)$ differs slightly in peak positions from the observed $I(K)$ for pure Cu. As a result $G_{\mathrm{CuCu}}(r)$ yields an interatomic distance $r_1 = 2.60$ A which is larger than that found in Cu ($r_1 = 2.50$ A), but is consistent with the interatomic distances found in the Cu_3Sn structure.

In determining the electron transport properties, particularly the thermoelectric parameter X, it could be expected that the positions of the peak maxima of the partials would greatly affect the predicted results. However, it would seem that the partials that can represent the Cu–Sn system, certainly as far as the transport phenomena are concerned, are by no means unique since both the neutron and X-ray predictions agree well with experiment (see Fig. 15). Even the total $I(K)$ of the alloys, when used within the framework of the substitutional model, are able to reproduce the electron transport properties in reasonable detail. The conclusion would be that the Faber–

Ziman model, within the framework of local potentials, can account sufficiently well for the observed features in the experimental results. This agreement could, however, be fortuitous, since a more complete approach would invoke energy dependence, particularly in the case of Cu, perhaps along the approach adopted by Meyer *et al.*[38] for the monovalent metals and alloys; but unfortunately where results for a polvalent metal like Sn are not at present forthcoming.

REFERENCES

1. Wagner, C. N. J., *Adv. X-Ray Analysis* **12**, 50 (1969).
2. Halder, N. C. and Wagner, C. N. J., *J. Chem. Phys.* **47**, 4385 (1967).
3. Keating, D. T., *J. Appl. Phys.* **34**, 923 (1963).
4. Enderby, J. E., North, D. M., and Egelstaff, P. A., *Phil. Mag.* **14**, 961 (1966).
5. Orton, B. R. and Williams, G. I., quoted in Ref. 4 (see Orton, B. R., Ph.D. Thesis, University of London, 1964).
6. Enderby, J. E., North, D. M., and Egelstaff, P. A., *Adv. Phys.* **16**, 171 (1967).
7. Wagner, C. N. J., Halder, N. C., and North, D. M., *Z. Naturf.* **24a**, 432 (1969).
8. Ashcroft, N. W. and Langreth, D. C., *Phys. Rev.* **156**, 685 (1967).
9. Enderby, J. E. and North, D. M., *Phys. Chem. Liquids* **1**, 1 (1968).
10. Kaplow, R., Strong, S. L., and Averbach, B. L., *Local Atomic Arrangement Studied by X-Ray Diffraction*, ed. by J. B. Cohen and J. E. Hilliard, Gordon and Breach, New York 1966.
11. Faber, T. E. and Ziman, J. M., *Phil. Mag.* **11**, 153 (1965).
12. Animalu, A. O. E. and Heine, V., *Phil. Mag.* **12**, 1249 (1965).
13. Wagner, C. N. J., " Theta–Theta Diffractometer with Stationary, Horizontal Sample Holder ", Technical Report No. 2 USAEC AT(30–1) 2560.
14. Wagner, C. N. J., Ocken, H., and Joshi, M. L., *Z. Naturf.* **20a**, 325 (1965).
15. Halder, N. C., Metzger, R. J., and Wagner, C. N. J., *J. Chem. Phys.* **45**, 1259 (1966).
16. Cromer, D. T. and Waber, J. T., *Acta Cryst.* **18**, 104 (1965).
17. Cromer, D. T., *Acta Cryst.* **18**, 17 (1965).
18. Sagel, K., *Tabellen zur Röntgenstrukturanalyse*, Springer Verlag, Berlin (1958).
19. Wagner, C. N. J., Technical Report No. 2, NSF GP 3213.
20. Ruppersberg, H., *Mem. Scient. Rev. Met.* **61**, 709 (1964).
21. North, D. M., and Wagner, C. N. J., " Temperature Dependence of the Interference Function and the Electronic Transport Properties of Liquid Tin " (to be published).
22. North, D. M., Enderby, J. E., and Egelstaff, P. A., *J. Physics C*, **1**, 1075 (1968).
23. Ziman, J. M., *Adv. Phys.* **13**, 89 (1964).

24. Roll, A. and Motz, H., *Z. Metallkunde* **48**, 435 (1957).
25. Pfannenschmid, O., *Z. Naturf.* **15a**, 609 (1960).
26. Hendus, H. and Knödler, H., *Acta Cryst.* **9**, 1036 (1956). (See Knödler, H., Dr. rer. nat. thesis, University of the Saar, Saarbrücken, Germany, 1958.)
27. Krebs, H., Hermsdorf, H., Thurn, H., Welte, H., and Winkler, L., *Z. Naturf.* **23a**, 491 (1968).
28. Ruppersberg, H., *Z. Naturf.* **24a**, 1034 (1969).
29. Pings, C. J. and Waser, J., *J. Chem. Phys.* **48**, 3016 (1968).
30. Wagner, C. N. J. and Halder, N. C., *Adv. Phys.* **16**, 241 (1967).
31. Animalu, A. O. E. (private communication).
32. Busch, G. and Güntherodt, H.-J., *Phys. Kond. Mat.* **6**, 325 (1967).
33. Busch, G. and Güntherodt, H.-J., Solvay Congress, Brussels, 1969.
34. Halder, N. C., North, D. M., and Wagner, C. N. J., *Phys. Rev.* **177**, 47 (1969).
35. Enderby, J. E. and Howe, R. A., *Phil. Mag.* **18**, 923 (1968).
36. Howe, R. A. and Enderby, J. E., *Phil. Mag.* **16**, 467 (1967).
37. Breuil, M. and Tourand, G., to be published in *Jour. Phys. Chem. Solids.*
38. Meyer, A., Nestor Jr., C. W. and Young, W. H., *Proc. Phys. Soc.* **92**, 446 (1967).